THE STRUCTURAL DESIGN OF TALL AND SPECIAL BUILDINGS
Struct. Design Tall Spec. Build. **17**, 117–132 (2008)
Published online 18 June 2007 in Wiley Interscience (www.interscience.wiley.com). **DOI**: 10.1002/tal.335

APPLICATION OF GPS TO MONITORING OF WIND-INDUCED RESPONSES OF HIGH-RISE BUILDINGS

HYO SEON PARK[1]*, HONG GYOO SOHN[2], ILL SOO KIM[1] AND JAE HWAN PARK[1]
[1] *Department of Architectural Engineering, Yonsei University, Seoul, Korea*
[2] *Department of Civil Engineering, Yonsei University, Seoul, Korea*

SUMMARY

A new monitoring system using GPS is introduced to measure wind-induced responses of high-rise buildings. In this paper, wind-induced responses of a long-period structure include relative lateral displacements, acceleration records, and torsional displacements at the top of a building. After comparing responses of a test model measured by GPS with responses obtained by the most commonly used laser displacement meters and accelerometers, the wind-induced responses of a 66-story high-rise building subject to the yellow dust storm were measured by the GPS-based monitoring system. Based on the field measurement, it is concluded that the complete motion history of a high-rise building can be monitored by GPS. Copyright © 2007 John Wiley & Sons, Ltd.

1. INTRODUCTION

Structural design of a high-rise building is defined as an iterative process of determining its structural systems and cross-sectional properties of structural elements so that the structural responses to all anticipated load combinations satisfy criteria for safety and serviceability as specified in the design codes. In the case of a high-rise building that has a relatively high slenderness ratio greater than 5·0 the quality of the structural design depends more on satisfying the serviceability criteria than those of safety (Park and Park, 1997).

Serviceability of high-rise buildings against lateral loads such as wind loads is evaluated in terms of two types of structural responses: lateral displacement and horizontal acceleration level. Excessive lateral displacement can cause structural problems as well as other diverse problems on non-structural elements such as damage to finishing materials, while excessive horizontal acceleration level can bring feelings of unpleasantness to building occupants. For these reasons various research studies have been conducted on methods of measuring and controlling relative lateral displacements and horizontal acceleration of high-rise buildings (Park *et al.*, 2002; Aldawod *et al.*, 2001).

Wind-induced lateral displacement is composed of static component and dynamic fluctuating component. The accelerometer method, which is most frequently used, has certain problems such as determination of appropriate integral constant for compound numerical integration for measuring static component as a part of horizontal displacement component (Loves *et al.*, 1995). Therefore, many researchers have recently been attempting direct measurement of horizontal displacements using GPS (Loves *et al.*, 1995; Nakamura, 2000; Çelebi, 2000; Tamura *et al.*, 2002; Breuer *et al.*, 2002; Kijewski and Kareem, 2003a, 2003b).

*Correspondence to: Hyo Seon Park, Department of Architectural Engineering, Yonsei University, 134 Shinchon-dong, Seoul 120749, Korea. E-mail: hspark@yonsei.ac.kr

Loves *et al.* (1995) measured horizontal displacement history of Calgary Tower against wind loads using GPS and analyzed the natural frequency based on such measurements. Çelebi (2000) measured horizontal displacement history of a 44-story building and verified that the natural frequency of 0·23 Hz as computed from such measurement coincided with the natural frequency as analyzed from the building's accelerometer study. Tamura *et al.* (2002) demonstrated that it was possible to directly measure actual displacements using GPS with publicized accuracy of ±1 cm +1 part per million (ppm) in cases when a building's natural frequency is less than 2 Hz and amplitude greater than 2 cm, and published the displacement history of a 108 m steel tower. Breuer *et al.*, (2002) measured displacement history and natural frequency of the Stuttgart TV tower against wind loads and suggested the usefulness of GPS in monitoring safety of high-rise buildings that are thin and long based on such GPS measurements.

Lateral load such as wind loads causes displacement as well as horizontal vibrations at the same time. Such horizontal vibrations can cause direct unpleasant feelings to the building's occupants and thus can be a more critical criterion of serviceability than horizontal displacement (Melbroune and Palmer, 1992). Horizontal acceleration of a building caused by wind loads is mostly measured using accelerometers as shown by Li *et al.* (2000), who measured a 70-story building's reaction against typhoon using accelerometers.

Building displacement measurements using GPS have been reported frequently, as mentioned above. However, no cases have been reported yet of horizontal acceleration measurement and building serviceability assessment based on GPS. Therefore, we can use a mixed approach for serviceability assessment of high-rise buildings against wind loads; that is, we can use GPS to measure horizontal displacements and use accelerometers to measure the horizontal acceleration level. However, for efficient serviceability assessment as well as monitoring of structural responses of high-rise buildings we need to develop a method of simultaneously measuring both horizontal displacements and horizontal acceleration.

In this paper, we verify feasibility of a GPS method for monitoring both horizontal displacement and horizontal acceleration of high-rise buildings that are subject to wind loads. Additionally, high-rise buildings that are subject to wind load, which is applied through planar non-uniformity, experience horizontal displacement accompanied by torsional displacement. Measurement of such torsional displacement has not yet been reported. In this paper, we introduce a method of monitoring comprehensive displacement history of high-rise buildings by measuring not only horizontal displacements but also torsional displacements.

For this purpose, we first used a fixed known position to measure accuracy of GPS receivers for horizontal displacement measurements. We then installed a GPS receiver, a laser displacement meter, and accelerometers on a physical test model that can vibrate horizontally so that the model's GPS measurements were compared against actual displacements as measured by the laser meter and actual acceleration as measured by the accelerometer. Finally, we installed two wind vanes and anemographs, two accelerometers, and two GPS receivers on a 66-story building to measure its responses against yellow dust storm.

2. GPS ACCURACY TEST

2.1 GPS receiver accuracy at a fixed position

In order to verify reliability of GPS measurement data we installed a GPS receiver at a fixed location and verified its horizontal component measurement accuracy by varying the baseline distances with respect to a base station. Here, for the sake of accurate observation we varied the baseline distance to 1 km and 4 km. Geometric errors in GPS arise from the geometric arrangement of four or more

DOI: 10.1002/tal

Table 1. Number of satellites observed and PDOP

Location	Observed satellites	PDOP
A (Baseline distance 1 km)	5	2·8–4
B (Baseline distance 4 km)	7	2·1–2·8

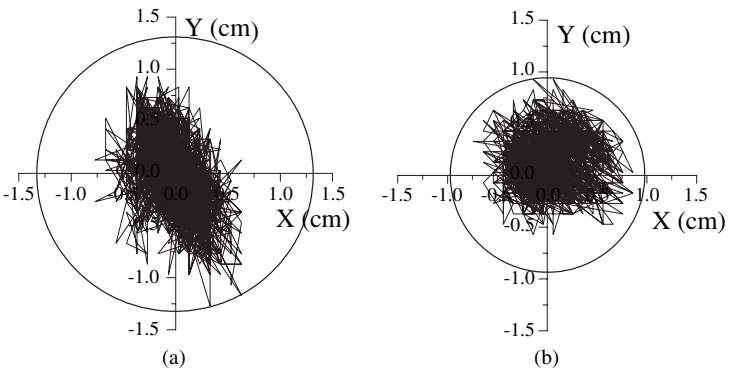

Figure 1. 40 min measurement of a fixed point with different baseline distances: (a) baseline distance 1 km; (b) baseline distance 4 km

observed satellites and are expressed as PDOP (position dilution of precision) values. Measurement data with PDOP of five or less can be trusted so that the smaller the PDOP value, the less the error. Measurements were taken at PDOP 3 or less in order to eliminate geometric error factors of GPS as much as possible. Also, in order to eliminate errors from multiple paths we performed our tests in a school ground where we had a large space. Measurement time at each baseline distance was 40 min each and the measured data were processed using the PPK (post-processed kinematic) method. The numbers of observed GPS satellites and PDOP for each baseline distance are shown in Table 1.

For the GPS accuracy test for each baseline distance we projected the three-dimensional displacement contour onto each coordinate to obtain two-dimensional displacements, which were then projected to each axis direction. The *X*–*Y* coordinate displacements are presented as in Figure 1 for each baseline distance. As a measure of maximum error, a circle with the maximum value of measured data as its radius is drawn in Figure 1. The error ranges of standard deviations of measured data using the Trimble 4700 system under 10 km baseline distances are horizontal 1 cm + 1 ppm and vertical 2 cm + 1 ppm. Actual displacements, means and standard deviations of displacement data measured for 40 min are as in Table 2. Standard deviations for 1 km baseline were *X*-axis 0·22 cm and *Y*-axis 0·34 cm, while those for 4 km were *X*-axis 0·26 cm and *Y*-axis 0·23 cm. This seems to be from the influence of PDOP and number of observed satellites in spite of longer baseline, as shown in Table 1. Thus, reliability of GPS data as processed with the PPK method has been verified as deviations not exceeding tolerable error ranges.

2.2 Structural responses using a physical model

We constructed a test model, as shown in Figure 2, that can vibrate horizontally in order to compare GPS measured displacements and accelerations against laser-measured displacements and accelerometer-measured accelerations. This physical model has a wooden board of 2·44 m × 1·24 m supported by six vertical D10 deformed rebars. On this model we installed a GPS receiver, servo-type

DOI: 10.1002/tal

Table 2. Accuracy test results for different baseline distances

Location:		A	C
Baseline distance:		1 km	4 km
Displacement range (cm)	*X*-axis	+0·63	0·93
		–0·77	0·74
	Y-axis	+0·93	0·96
		–1·27	0·57
Average displacement (cm)	*X*-axis	–0·01	0·00
	Y-axis	–0·02	0·12
Standard deviation (cm)	*X*-axis	0·22	0·26
	Y-axis	0·34	0·23

Figure 2. Experimental model

accelerometers, and a laser displacement meter as shown in Figure 3. Also, we installed braces on the vertical elements with a deformed rebar in order to prevent *Y*-axis vibration when the model vibrates in the *X*-axis direction. Furthermore, we installed rubber pads at all connection joints to reduce energy loss at such points during free vibration of the model.

Measurements were taken at 5 Hz, which is more than twice the natural frequency of the structure. GPS displacement history and laser displacement history of the model for an initial displacement of 4 cm are compared as in Figure 4. Here, we can see that the displacements using GPS coincide quite well with actual displacements using a laser meter for displacement amplitude of greater than 1 cm.

Comparison of acceleration as differentiated from measured displacements using GPS and laser displacement meter against actual measured acceleration using servo-type accelerometer is as in Figure 5. The GPS and laser meter accelerations are computed by numerically differentiating displacement values of three consecutive points of $t - \Delta t$, t, $t + \Delta t$ using the Equation (1) to obtain $\omega(t)$ at time t, and then performing numerical differentiation again in a similar manner to obtain acceleration.

DOI: 10.1002/tal

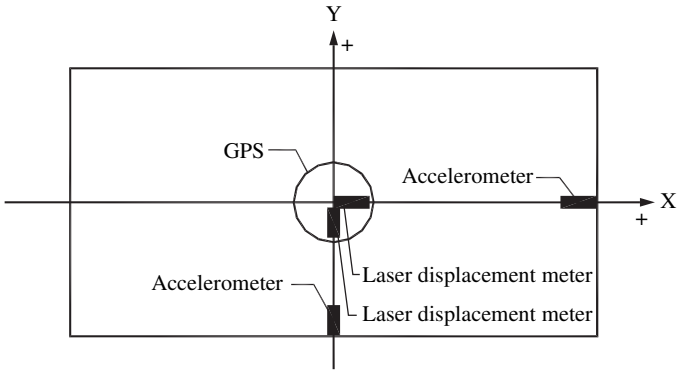

Figure 3. Measurement devices and data acquisition coordinate convention

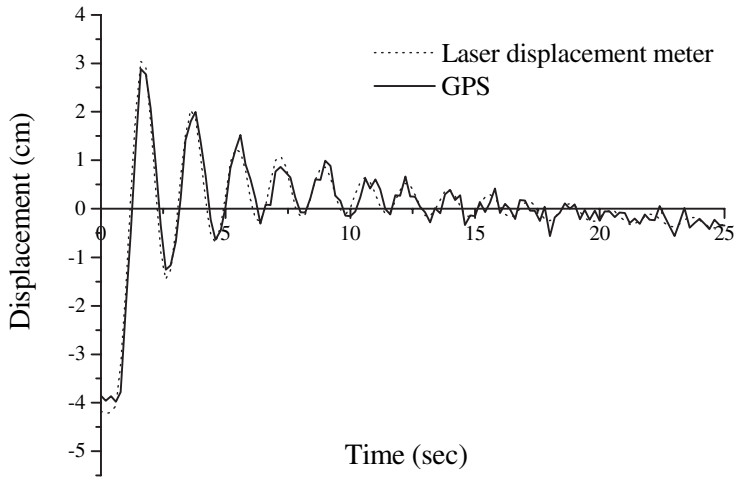

Figure 4. Displacement measurement by GPS and laser displacement meter

$$v(t) = \frac{1}{2}\left(\frac{x_{t+\Delta t} - x_t}{\Delta t} + \frac{x_t - x_{t-\Delta t}}{\Delta t}\right) \tag{1}$$

As shown in Figure 5, acceleration obtained using a GPS receiver coincide well with actual acceleration measured with an accelerometer. We then performed fast Fourier transform (FFT) on acceleration data using GPS, laser displacement meter, and accelerometer, respectively, to compute the natural frequency of the physical model. The three results provide an identical natural frequency of 0·6 Hz, as shown in Figure 6.

3. ACTUAL MEASUREMENT OF WIND-INDUCED RESPONSES IN A 66-STORY HIGH-RISE BUILDING

3.1 Building for measurement

The building we measured is a 66-story mixed-use high-rise building with base plane dimensions of 42·6 m × 35·1 m, as shown in Figure 7. Its height to the heliport, where the GPS equipment was installed, is 233·9 m and the slenderness ratio is 6·63 (Figure 8).

DOI: 10.1002/tal

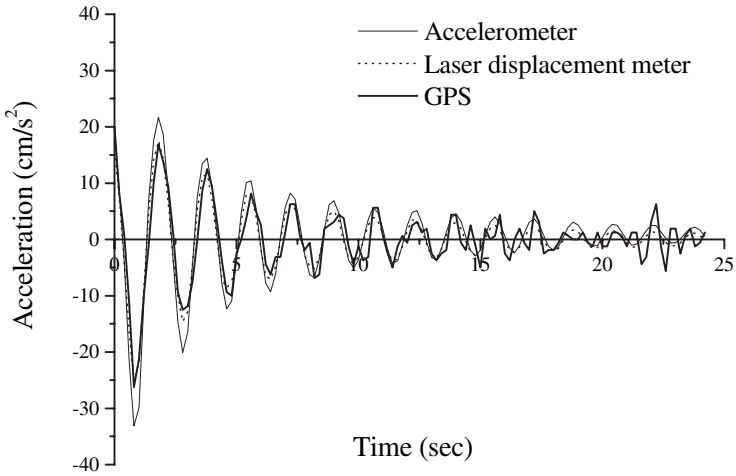

Figure 5. Acceleration measurement by GPS, laser displacement meter, and accelerometer

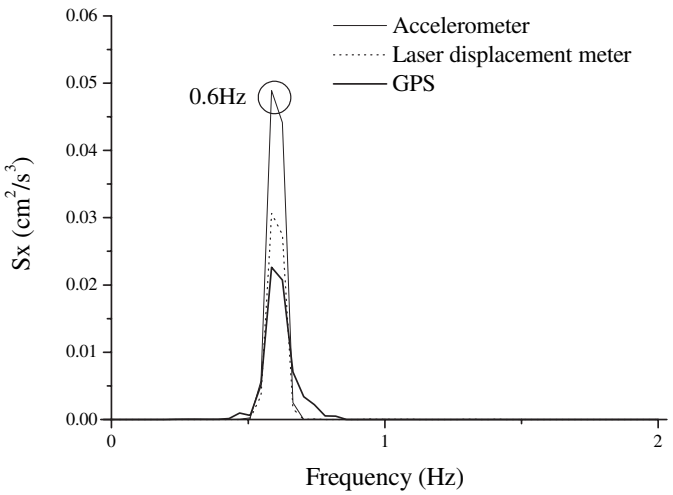

Figure 6. Natural frequency comparison by GPS, laser displacement meter, and accelerometer

3.2 Measurement system

We employed two GPS receiver antennas for measuring lateral and torsional displacements of the building, two wind vanes and anemographs for measuring wind direction and speed, and two servo-type accelerometers for measuring acceleration response. We set the lengthwise direction of the building as the *X*-axis as the dimensional convention for data acquisition. Equipment installation was as shown in Figure 7.

The wind vane and anemometer were used to measure wind speed and direction. The measurable range of wind speed was 0–60 m/s, with a wind speed accuracy of ±0·3 m/s and wind direction accuracy of ±3°. Anemographs were installed to measure wind speed and direction at positions A and B on the heliport, as shown in Figure 7. One position was at the outer end and the other inside of the heliport in consideration of possible wind turbulence impact. Mobile GPS receivers were placed at

DOI: 10.1002/tal

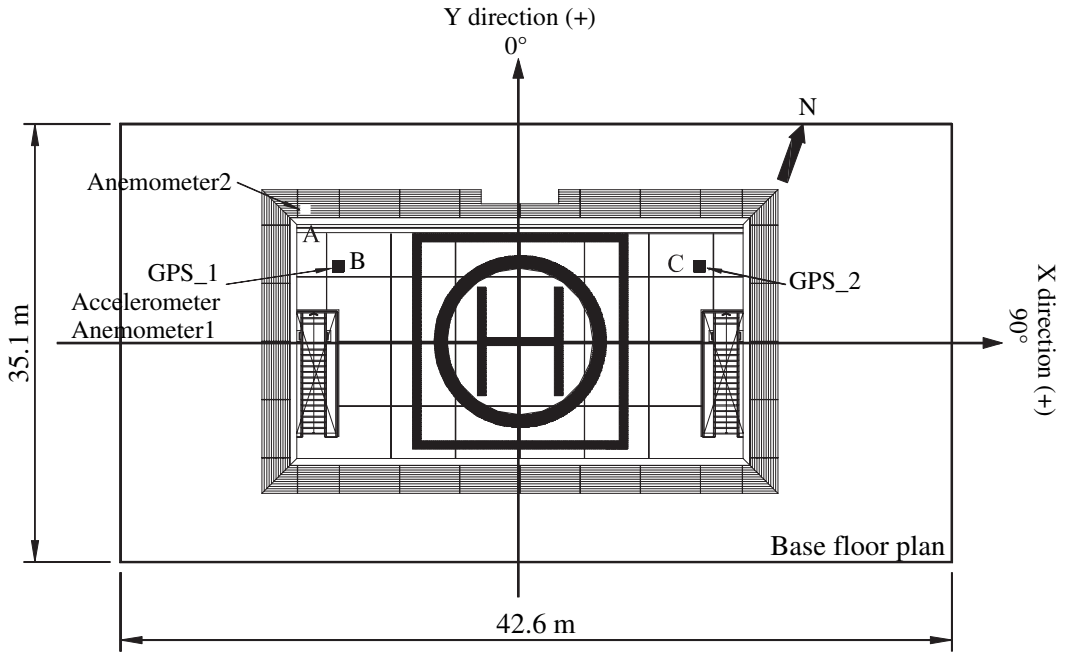

Figure 7. Measurement devices and coordinate convention

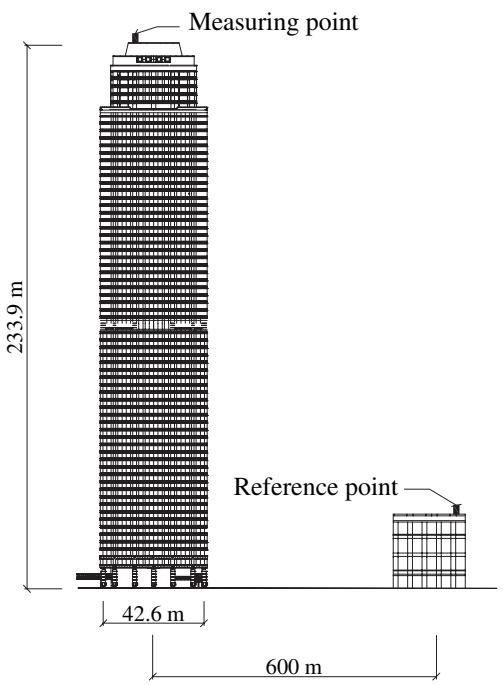

Figure 8. A 66-story building for full-scale test

DOI: 10.1002/tal

the same locations as the anemometers. The GPS base station as the reference point was installed on the roof of a five-story apartment building some 600 m away from the measurement building, as shown in Figure 8, to ensure no lateral displacement.

Monitoring of the building response against wind loads were performed for approximately one year during 2002. In this paper we performed analysis of its response to yellow dust storm on March 22 and to a typhoon during August 2002.

3.3 GPS displacements

Since the building displacement measured with GPS could be obtained from comparison of reference point coordinates and measured coordinates, the reference point coordinates for relative displacement measurement were set before the *de facto* experiment at a time period with wind speed less than 4·3 m/s. Displacement measurements were performed on a day when the wind speed exceeded 10 m/s with yellow dust storm blowing. The 10 min measurement of displacement history on top of this very high building is displayed in three-dimensional displacement loci in global coordinates as shown in Figure 9. These loci were projected on to a two-dimensional plane and the *X*-axis and *Y*-axis components of displacements expressed together with wind speed and direction data are as shown in Figure 10. As shown in the figure, the 10 min displacement had an *X*-axis range of −11·7 to 20·9 mm and mean of 3·0 mm, and a *Y*-axis range of 31·8–61 mm and mean of 44·0 mm. Each directional mean displacement can be construed as a static component of the displacement while its dynamic component can be verified to be approximately 30 mm, as seen in Figure 10. The average wind speed during the 10 min period of the building top displacement measurement using GPS was 12·29 m/s with the prevalent wind direction of 260° (Figure 10).

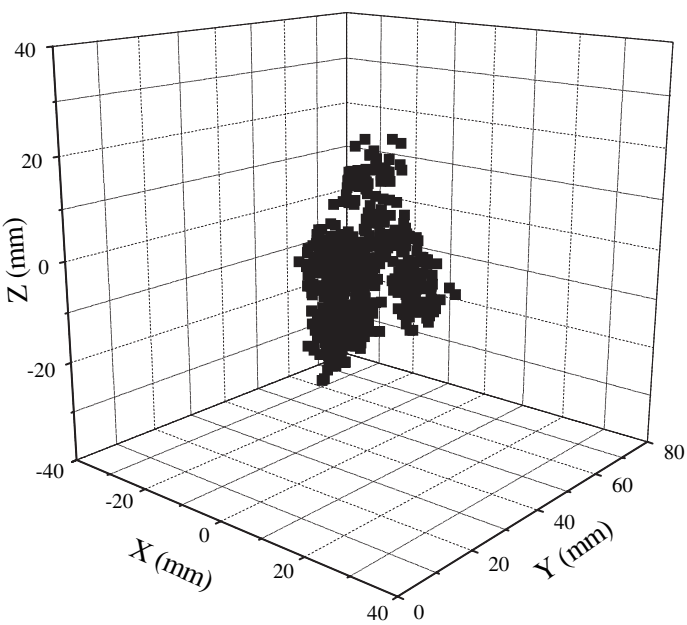

Figure 9. Three-dimensional movement measured by GPS

DOI: 10.1002/tal

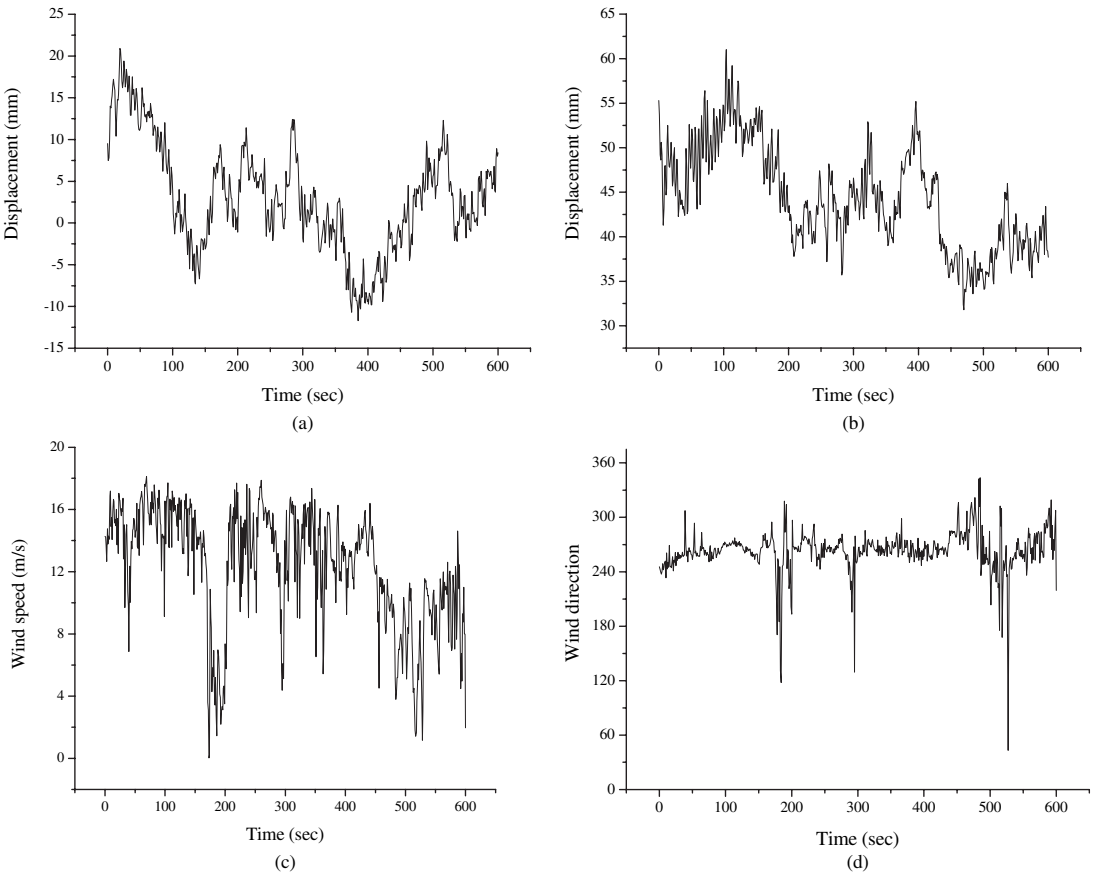

Figure 10. Measured displacements, wind direction, and wind speed: (a) time history of movement of a 66-story building in *X*-direction; (b) time history of movement of a 66-story building in *Y*-direction; (c) wind speed; (d) wind direction

3.4 Acceleration measured with GPS and accelerometer

We installed two servo-type accelerometers at position B as shown in Figure 7 in order to compare computed acceleration from GPS-measured displacement data against acceleration from accelerometers. We performed two-stage differentiation of *X*-axis and *Y*-axis direction GPS-measured displacements of Figure 10 to obtain accelerations. For more detailed comparison, we present accelerations for a 10 s interval as measured with accelerometers at 5 Hz and those as measured with GPS at 1 Hz in Figure 11.

Also, exploring the relationship between wind direction and acceleration level, we see that when the main wind direction is between 260° and 270°, the *Y*-axis acceleration (Figure 12b), which is perpendicular to wind direction, is greater than that of *X*-axis acceleration (Figure 12a). This satisfies Equation (2), suggested by NRCC (1996) as a condition for cross-windward acceleration to exceed windward acceleration, as well as Equations (3) and (4) suggested in the Japanese criteria (AIJ, 1991, 1996):

$$\frac{\sqrt{WD}}{H} = \frac{\sqrt{35{\cdot}1 \times 42{\cdot}6}}{233{\cdot}9} = 0{\cdot}17 < 1/3 \tag{2}$$

DOI: 10.1002/tal

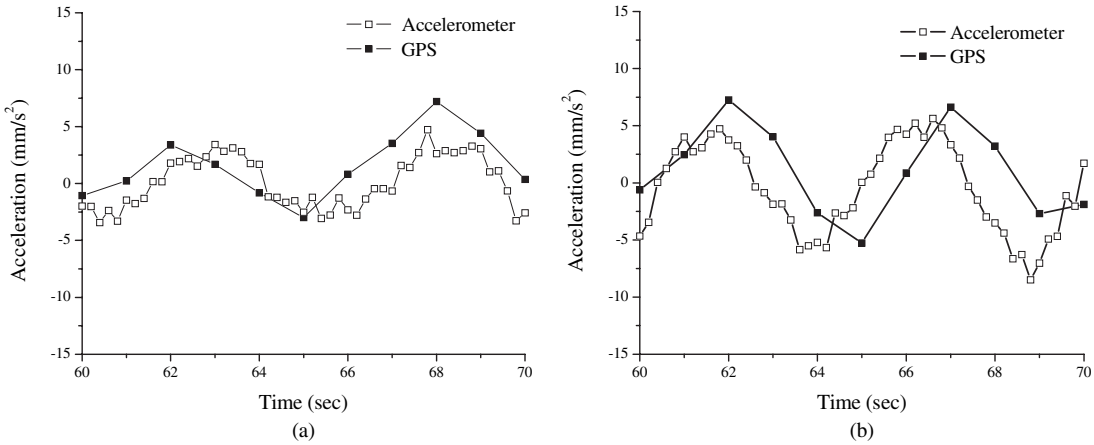

Figure 11. Detailed comparison of accelerations form GPS and accelerometers: (a) *X*-axis acceleration; (b) *Y*-axis acceleration

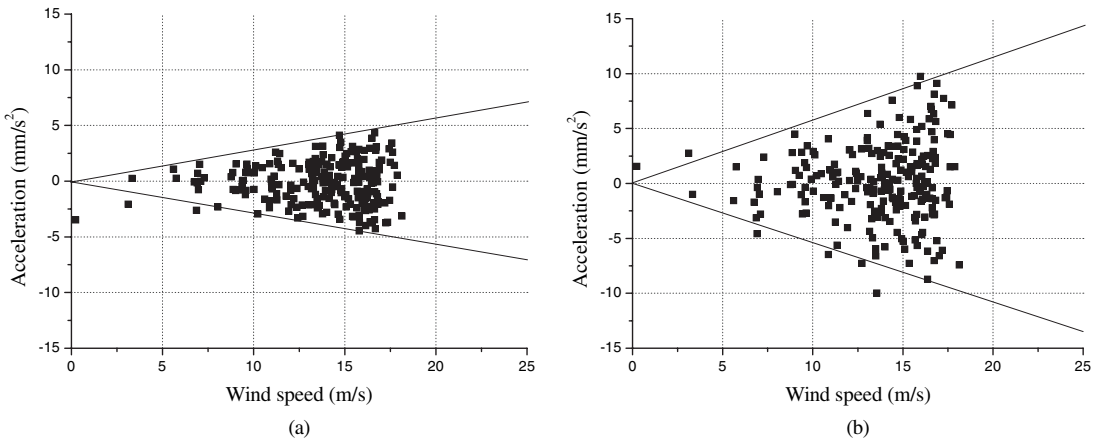

Figure 12. Measured acceleration range and wind speed: (a) *X*-axis acceleration; (b) *Y*-axis acceleration

$$\frac{H}{\sqrt{WD}} = 6 \cdot 05 > 3 \cdot 0 \tag{3}$$

$$\frac{f_n \sqrt{WD}}{UZ} = \frac{0 \cdot 125 \times \sqrt{(WD)}}{35} = 0 \cdot 23 < 0 \cdot 4 \tag{4}$$

Here, *W*, *D* and *H* refer to *X*-axis and *Y*-axis dimensions of the building base plane and its height. Also, f_n signifies the building's natural frequency. The first mode natural frequencies of the high-rise building using accelerometers and GPS coincide as shown in Figure 13 and these results are tabulated in Table 3.

DOI: 10.1002/tal

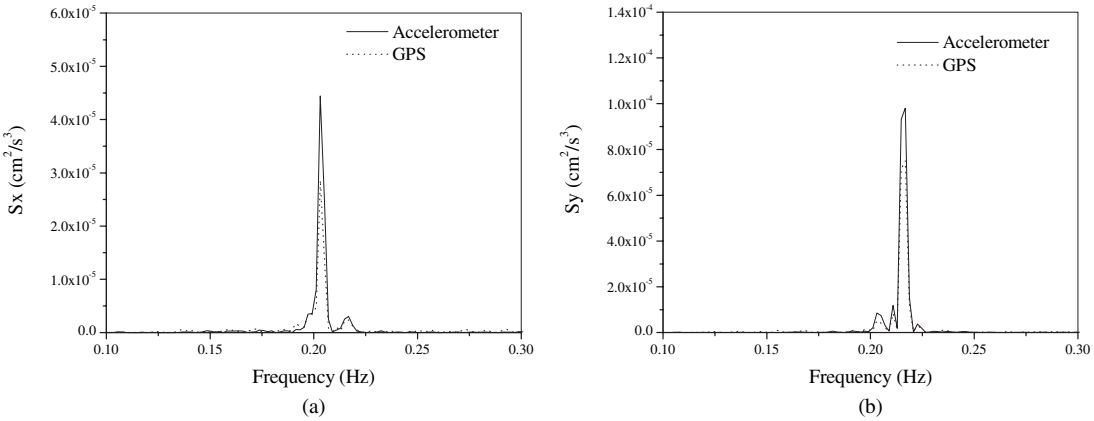

Figure 13. Fundamental natural frequency plot: (a) *X*-axis frequency; (b) *Y*-axis frequency

Table 3. Fundamental natural frequencies from GPS and accelerometers

	Natural frequency (Hz)	
Axis	GPS	Accelerometer
X	0·203	0·203
Y	0·215	0·215

3.5 Torsional displacement

High-rise building displacements consist of horizontal displacement of *X*-axis and *Y*-axis as well as torsional displacement. In order to measure torsional displacement we installed GPS_1 at point B of Figure 7 and GPS_2 at a distance of 16 182 mm from point B. We denote GPS_1 coordinates as (*X*1, *Y*1) and GPS_2 coordinates as (*X*2, *Y*2) so that their installation coordinates are (0 mm, 0 mm) for GPS_1 and (16 182 mm, 0 mm) for GPS_2. The torsional displacement $\theta(t)$ at time t can be computed using Equation (5) and these coordinate values:

$$\theta(t) = \tan^{-1}\left(\frac{\Delta Y(t)}{\Delta X(t)}\right) = \left(\frac{Y_2(t) - Y_1(t)}{X_2(t) - X_1(t)}\right) \tag{5}$$

The *X*-axis displacement differential $\Delta X(t)$ and *Y*-axis displacement differential $\Delta Y(t)$ between GPS_1 and GPS_2 were measured for 30 min from 17:10 to 17:40 on 2 September 2002. The computed torsional displacement of the building using Equation (5) is as in Figure 14.

In general a slab in a building is assumed to be a rigid diaphragm with infinite stiffness. Therefore, the distance between two GPS stations may maintain 16 812 mm during the measurement period. The error distance between two GPS stations during the measurement period can be computed using Equation (6) as follows:

$$\Delta l(t) = \sqrt{\Delta X(t)^2 + \Delta Y(t)^2} - 16812 \tag{6}$$

Using this distance error we can indirectly evaluate the accuracy of the GPS displacement measurement system. The computed distance error between two GPS stations during the 100 s of measurement is as in Figure 15 and was maintained within a 5 mm range.

DOI: 10.1002/tal

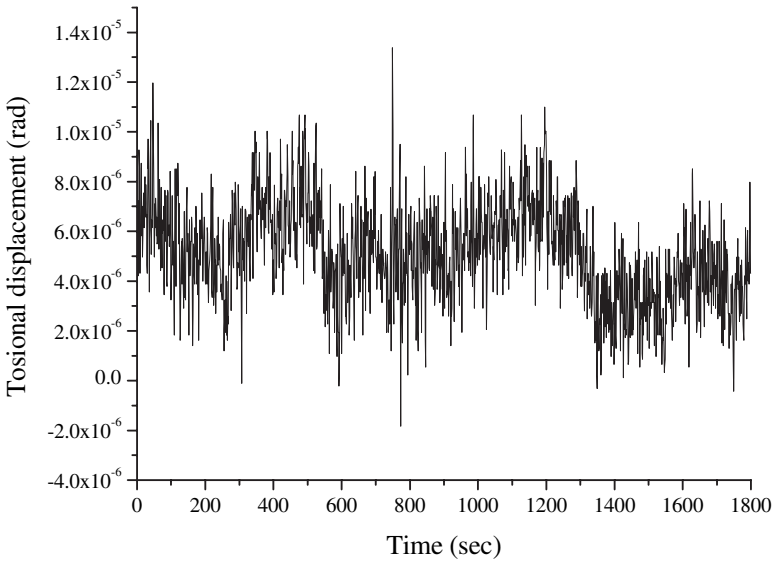

Figure 14. Torsional displacement

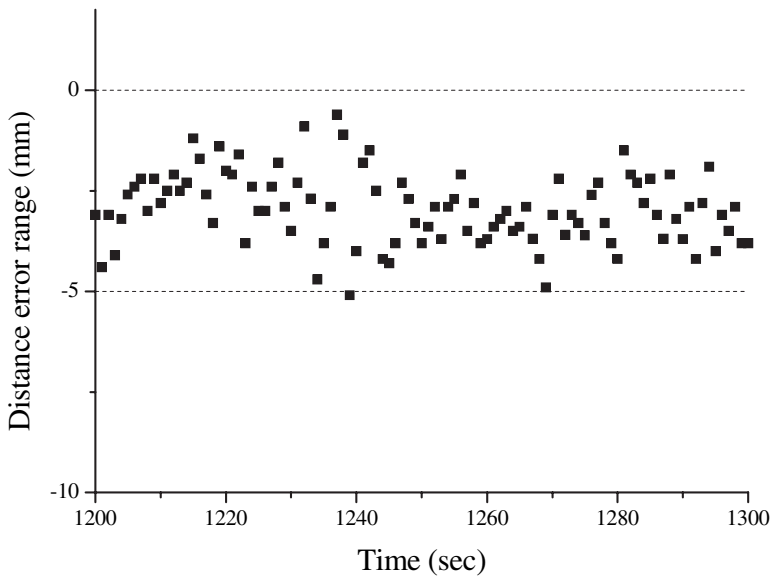

Figure 15. Computed error in length between points A and B

4. SERVICEABILITY ANALYSIS OF 66-STORY HIGH-RISE BUILDING

Although serviceability of a high-rise building is evaluated in terms of horizontal displacement and horizontal acceleration level, the criterion that building occupants feel personally is the building's vibration level due to wind loads. In this paper we compared and analyzed the building's serviceability in terms of acceleration level during a typhoon as measured from 06:00 to 18:00 on 31 August 2002 using GPS and accelerometers.

DOI: 10.1002/tal

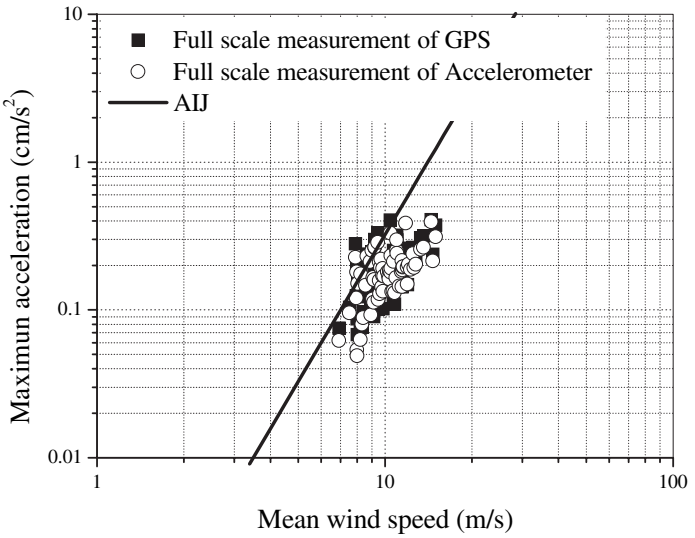

Figure 16. Relation between wind speed and acceleration response in *Y*-direction

4.1 Estimation of vibration level

Since this building's acceleration response of cross-windward direction is greater than that of the windward direction, we used *Y*-axis acceleration for assessment of serviceability. Figure 16 presents a comparison of maximum acceleration response on average wind speed of 10 min measured with GPS and accelerometers against the forecast equation (AIJ, 1991) in the Japanese habitability evaluation guideline. As seen in the figure, the maximum computed acceleration values from the two measurement techniques are either similar to or less than that of the estimation equation.

The acceleration responses at the top of the building as measured with accelerometers and GPS in terms of the relationship between the mean wind speed and the root mean square (RMS) acceleration for the 10 min period is as presented in Figures 17 and 18, respectively. These are expressed as Equations (7) and (8) via regression.

$$\sigma_{y,acc} = 0{\cdot}0051\overline{V}^{1{\cdot}5251} \tag{7}$$

$$\sigma_{y,gps} = 0{\cdot}0052\overline{V}^{1{\cdot}5076} \tag{8}$$

Here, $\sigma_{y,acc}$, $\sigma_{y,gps}$, and $\overline{V}$ represent RMS acceleration from accelerometer, RMS acceleration from GPS and the 10-minute mean wind speed, respectively. The building's wind response to wind load may be estimated using the above regression equations.

4.2 Serviceability evaluation

In this paper we used Equation (9), proposed by Li (2000), to compute allowed RMS acceleration by return period on the 10 min mean wind speed to evaluate the building's serviceability:

$$\sigma_R(m/s^2) = \left(0{\cdot}68 + \frac{\ln R}{5}\right)\exp(-3{\cdot}65 - 0{\cdot}41\ln n) \tag{9}$$

Here, n and R represent natural frequency and representation cycle, respectively.

DOI: 10.1002/tal

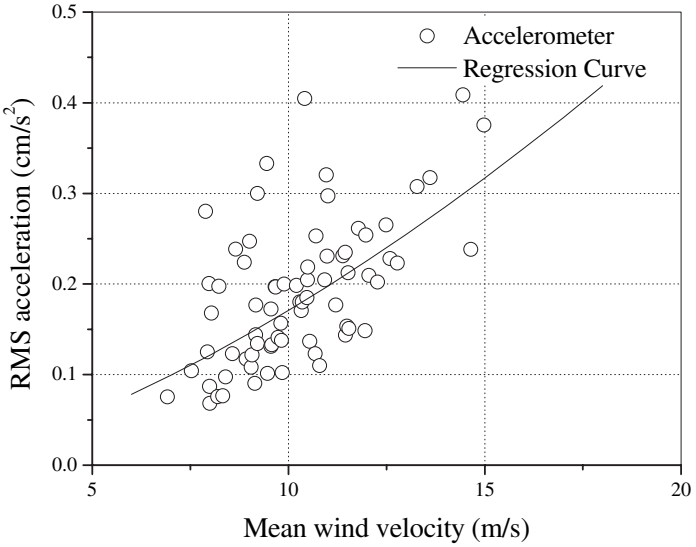

Figure 17. Relation between RMS acceleration from accelerometer and wind speed in *Y*-direction

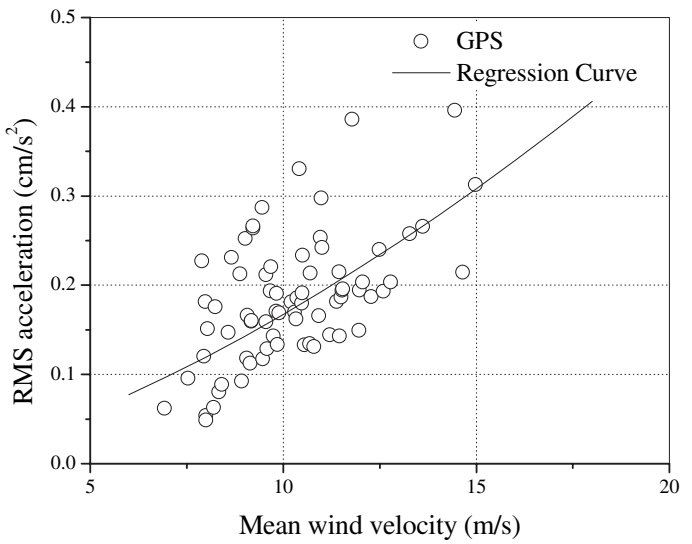

Figure 18. Relation between RMS acceleration from GPS and wind speed in *Y*-direction

In order to compare with the allowed RMS acceleration value from Equation (9), we express RMS acceleration levels from GPS and accelerometer of Equations (7) and (8) using the Korean Standard Design Loads for Buildings (AIK, 2000) as return period function as in Equations (10) and (11).

$$\sigma_{y,acc} = 0{\cdot}0051\left(23{\cdot}47 - 3{\cdot}9\ln\left(\ln\frac{R}{R-1}\right)\right)^{1{\cdot}5251} \tag{10}$$

DOI: 10.1002/tal

Table 4. RMS accelerations based on Equations (9), (10), and (11) by return period

Return period R (years)	σ_{acc}, Equation (10) (cm/s^2)	σ_{gps}, Equation (11) (cm/s^2)	σ_R, Equation (9) (cm/s^2)
1	0·5739	0·5542	3·2528
5	0·8813	0·8470	4·7926
10	1·0190	0·9777	5·4557
20	1·1573	1·1088	6·1189
30	1·2396	1·1867	6·5068
40	1·2988	1·2427	6·7820
50	1·3452	1·2865	6·9955
60	1·3834	1·3227	7·1699
70	1·4160	1·3535	7·3174
80	1·4444	1·3803	7·4452
90	1·4696	1·4041	7·5578
100	1·4922	1·4255	7·6586

$$\sigma_{y,gps} = 0{\cdot}0052\left(23{\cdot}47 - 3{\cdot}9\ln\left(\ln\frac{R}{R-1}\right)\right)^{1{\cdot}5076} \tag{11}$$

Accelerations measured with GPS and accelerometers and the allowed value from Equation (9) are presented as in Table 4. As may be known from Table 4, since the estimated acceleration values using both measurement methods do not exceed the allowed values from Equation (9), the subject building for measurement satisfies the serviceability criteria for its occupants.

5. CONCLUSIONS

In this paper we introduced a method of monitoring horizontal displacement, torsional displacement and acceleration in high-rise buildings using GPS. Using a fixed point we tested the accuracy of GPS receivers for horizontal displacement measurement. We also installed a GPS receiver, a laser displacement meter, and accelerometers on a physical test model, and compared measured displacement and acceleration using GPS against actual displacement and acceleration using a laser meter. The results show that GPS-measured displacement and acceleration are similar to those from laser meter and servo-type accelerometer in cases of vibration amplitude greater than 1 cm.

Finally, we installed two wind vanes and anemometers, two accelerometers, and three GPS receivers on an actual 66-story high-rise building to measure and analyze the building's response to yellow dust storm and typhoon. We were able to measure horizontal displacement in terms of static displacement component and dynamic variable displacement component, while torsional displacement was also measured to define completely the building's movement under wind load. Additionally, we verified that the building's serviceability under wind load satisfies allowed values of RMS acceleration and maximum acceleration.

ACKNOWLEDGEMENTS

This work was supported by a Korea Research Foundation grant (KRF-2001-042-E00137).

DOI: 10.1002/tal

REFERENCES

Aldawod M, Samali B, Naghdy F, Kwok KCS. 2001. Active control of along wind response of tall building using a fuzzy controller. *Engineering Structures* **23**(11): 1512–1522.

AIJ (Architectural Institute of Japan). 1991. *Guidelines for the Evaluation of Habitability to Building Vibration*. AIJ: Tokyo.

AIJ (Architectural Institute of Japan). 1996. *Recommendations for Loads on Buildings*. AIJ: Tokyo.

AIK (Architectural Institute of Korea). 2000. *Standard Design Loads for Buildings*. AIK: Seoul.

Breuer P, Chmielewski T, Górski P, Konopka E. 2002. Application of GPS technology to measurement of displacements of high-rise structures due to weak winds. *Journal of Wind Engineering and Industrial Aerodynamics* **90**: 223–230.

Çelebi M. 2000. GPS in dynamic monitoring of long-period structures. *Soil Dynamics and Earthquake Engineering* **20**: 477–483.

Kijewski T, Kareem A. 2003a. The height of precision. *GPS World* September: 20–34.

Kijewski T, Kareem A. 2003b. GPS for monitoring the dynamic response of tall buildings: experimental verification and full-scale application. In *Proceedings of 2003 Structures Congress*, ASCE, Seattle, 29 May–1 June.

Li QS, Wong CK, Fang JQ, Jeary AP, Chow YW. 2000. Field measurements of wind and structural responses of a 70 story tall building under typhoon conditions. *Structural Design of Tall Buildings* **9**: 325–342.

Loves JW, Teskey WF, Lachapelle G, Cannon ME. 1995. Dynamic deformation monitoring of tall structure using GPS technology. *Journal of Surveying Engineering* **121**(1): 35–40.

Melbroune WH, Palmer TR. 1992. Acceleration and comfort criteria for buildings undergoing complex motions. *Journal of Wind Engineering and Industrial Aerodynamics* **41**: 105–116.

Nakamura SI. 2000. GPS measurements of wind induced suspension bridge girder displacement. *Journal of structural engineering, ASCE* **126**(12): 1413–1419.

NRCC (National Research Council of Canada). 1996. *Commentary B: Wind Loads—User's Guide*. NBC 1995 Structural Commentaries, Canadian Commission on Building and Fire Codes, Part 4: Ottawa.

Park HS, Park CL. 1997. Drift control of high-rise buildings with unit load method. *Structural Design of Tall Buildings* **6**: 23–35.

Park HS, Hong KP, Seo JH. 2002. Drift design of steel-frame shear-wall systems for tall buildings. *Structural Design of Tall Buildings* **11**: 35–49.

Tamura Y, Matsui M, Pagnini LC, Ishibashi R, Yoshida A. 2002. Measurement of wind-induced response of buildings using RTK-GPS. *Journal of Wind Engineering and Industrial Aerodynamics* **90**: 1783–1793.

DOI: 10.1002/tal